Drop Axis Ratios from a 2D Video Disdrometer

MERHALA THURAI AND V. N. BRINGI

Colorado State University, Fort Collins, Colorado

(Manuscript received 14 October 2004, in final form 28 January 2005)

ABSTRACT

Results from an experiment to measure the drop shapes using a 2D video disdrometer (2DVD) are reported. Under calm conditions, drops were generated from a hose located on a bridge 80 m above ground, this height being sufficient to allow drop oscillations to reach a steady state. The disdrometer data had to be carefully processed so as to eliminate the drops mismatched by the instrument and to remove the system spreading function. The total number of drops analyzed was around 115 000. Their axis ratio distributions were obtained for diameters ranging from 1.5 to 9 mm. The mean axis ratio decreases with increasing drop diameter, in agreement with the upper bound of the Beard and Chuang equilibrium shape model. The inferred mode of oscillation appears to be dominated by the oblate–prolate axisymmetric mode for the diameter range of 1.5 to 9 mm.

The mean axis ratio agrees well with two empirically fitted formulas reported in earlier studies. In addition, a linear fit was applied to the data for radar applications relating to rain retrievals from dual-polarization measurements. The 2DVD data taken in moderate stratiform rain were also analyzed in a similar way and the results agree with the artificially generated drop experiment, at least up to 4 mm. No data for larger diameters were available for stratiform precipitation. Finally, the fall velocity was examined in terms of drop diameter. The results closely follow an empirical formula fitted to the Gunn and Kinzer data as well as the Beard and Pruppacher data including a slight decrease in the terminal velocity with a diameter beyond 7 mm.

1. Introduction

It is well known that raindrops take on nearly oblate-spheroidal shapes, with their axis of symmetry aligned closely to the vertical and, furthermore, that the degree of oblateness has a monotonic dependence on the drop size. Polarization radars make use of this oblateness to measure the difference in backscatter reflectivity and the propagation phase. Drop shapes therefore play a crucial role in retrieving the drop size distribution (DSD) of the raindrops and the subsequent estimation of rainfall rates from the polarization radar measurements. More specifically, the derivation of DSD from the measured polarization requires as its key input parameter, the axis ratio as a function of raindrop diameter. A small error in the axis ratio can lead to significant errors in the estimated DSD and rainfall rates (Bringi and Chandrasekar 2001, chapter 7).

Corresponding author address: Dr. V. N. Bringi, Electrical and Computer Engineering, Colorado State University, Fort Collins, CO 80523-1373.
E-mail: bringi@engr.colostate.edu

The situation is further complicated by the fact that the drops oscillate as they fall and hence it may not be appropriate to assume the equilibrium shapes for the DSD derivation. Indeed, drop oscillation has been the subject of many studies, ranging from wind tunnel and other laboratory measurements to field studies in natural rain using ground-based and airborne instruments (see chapter 10 of Pruppacher and Klett 1997). Moreover, for radar applications, there have been focused studies using differential reflectivity (Z_{dr}) and Joss-type disdrometer, which have specifically recommended empirical modifications to the equilibrium drop shapes. The earliest and the most quoted study involved a high-resolution radar (Goddard et al. 1994a) that showed that the theoretical results of Pruppacher and Pitter (1971) had to be modified in order to improve the agreement between the computed Z_{dr} and the measured Z_{dr} (Goddard et al. 1982; Goddard and Cherry 1984). Since then, the theoretical modeling of equilibrium shapes has been improved and the resulting computations have been compared with experimental data. Most studies conclude that the drop oscillations result in effective mean shapes that are more spherical than

the equilibrium shapes for diameters less than 4 mm (Pruppacher and Klett 1997).

Drop shapes are not only important in rain radar remote sensing but also for propagation studies relating to satellite and terrestrial communication systems operating at microwave frequencies and above. Effects such as depolarization and differential attenuation can be estimated properly only if drop shapes are accurately known (Allnutt 1989, chapters 4 and 5).

With these requirements in mind, and with the various formulas that are now available in the literature that empirically relate the axis ratio to drop diameter, an experiment was undertaken to assess the accuracy of these relationships. Under calm conditions, water was sprayed at a height of 80 m from a bridge and the characteristics of the drops were recorded using a two-dimensional video disdrometer (2DVD), which determines the shapes and velocities of the particles falling through an aperture. The fall distance of 80 m was considered to be large enough for the drops to reach not only their terminal velocities but also steady-state oscillations. We report here the recorded data, their analyses, and compare the resulting axis ratios with previously published work. The drop diameters ranged up to 9.5 mm, thus enabling the axis ratio distributions of large drops to be determined. The results are also compared with the analyses of data taken during moderate stratiform precipitation events in a midlatitude location (Tokyo, Japan) using the same instrument model as the bridge experiment.

2. The 80-m bridge experiment

a. Instrumentation

The 2DVD is a fast imaging system with a 10 cm by 10 cm rectangular sensing area that images each particle (hydrometeor) falling through it. It is equipped with two high-speed line scan cameras with orthogonal projections. Each line scan camera will yield shape information on a plane and, from the images on the orthogonal planes (giving front view and side view of the particles), it is possible to obtain the three-dimensional shape information. This will provide the equivalent drop shape and the equivalent diameter along with the drop oblateness, which is the ratio of the height of the particle to its width from the widest scan line. Even if the particle has a horizontal velocity (which will result in a distorted shape), their estimated height and the width will not be changed and hence their estimated oblateness will not be affected (but will have an apparent canting angle). However, when the particles truly have a canting angle, their estimated width will be decreased and their height increased, resulting in a higher estimation of oblateness. This is considered in more detail by Kruger and Krajewski (2002). Figure 12 in their article shows that for a 5-mm particle diameter, a canting angle of $\pm 5^\circ$ can give rise to a bias of 1%. However, our experiment was conducted during calm atmospheric conditions and hence this effect is believed to be insignificant.

Calibration is performed using precisely machined spheres—that are dropped through the aperture—and determining their oblateness. The accuracy of the measured axis ratio depends on the camera resolution (horizontal resolution at the center of the measuring area is 0.152 mm and the lowest vertical resolution is 0.195 mm at 10 m s^{-1} fall speed); in the usual mode, the axis ratio is recorded to within an accuracy 0.01. Details of the instrument and calibration procedure are given in Randeu et al. (2002), Schönhuber et al. (1997), and Kruger and Krajewski (2002).

The light sources used for the two views generate "light sheets" that are separated by a precisely (and optimally) set distance. By matching the shadows of the hydrometeors from the upper and the lower sheets and by timing their fall, their vertical velocities are estimated (as well as their horizontal velocities). This is done independent of the axis ratio measurements. However, the hydrometeors can be mismatched at times, especially during intense events, but these can be identified from their incorrect estimation of the fall speeds and eliminated from data analyses, as will be illustrated later in section 2c.

b. The 80-m fall experiment

A railroad bridge (Jauntal Bridge in Carinthia, Austria) was selected for the experiment because of ease of access and availability of continuous water supply at the bridge and electric power at the bottom. An open water hose between the slats of a pedestrian walkway on the bridge generated a continuous stream that after around a 5-m fall became a column of drops simulating an artificial "rain" shaft. There were no obstructions in the vicinity of the rain shaft. The Jauntal Bridge spans a valley with a river running below and the 2DVD instrument was placed on the bank of the river. The data were collected over a period of 3 days in very light wind conditions (< 1 m s^{-1}). The instrument was calibrated a number of times each day. The 80-m fall is considered sufficient to produce steady-state oscillations and terminal velocities occurring in natural precipitation even though the drop size distribution and rain rates are not representative of realistic rain events.

c. Problems associated with mismatched drops

It has been frequently noticed that during heavy rain, there arises significant problems due to "mismatched" drops, that is, drops that are wrongly matched by cameras A and B of the video disdrometer. The mismatch will result in incorrect estimates of shapes and velocities. These can be recognized from the velocity–diameter plots as having velocities well outside the expected velocities for the corresponding diameters. Kruger and Krajewski (2002) illustrate this problem in their Fig. 8a, marked as outliers in their data. To overcome this artifact, a recommended velocity-based filter was applied to the data, which removes all drops lying outside the range:

$$|v_{\text{measured}} - v_A| < c\, v_A,$$

where v_A represents the formula given in Atlas et al. (1973), and c is a constant less than unity. Previously published work (e.g., Kruger and Krajewski 2002; Tokay et al. 2001) recommended the value of c to be around 0.4, which has been applied in this study. While such velocity-based filtering will modify the drop size distribution for very small drops, it is not expected to affect the drop shapes or the mean velocity. Figure 1a shows the two limits superimposed on the logarithmic intensity contour of the number of drops on a velocity–diameter plot. The equivalent drop axis ratio with and without the filtering is compared in Figs. 1b,c. As shown, it gives rise to a sharper intensity plot, particularly removing the incorrect (and impossible) axis ratios in the case of small drops. The resulting number intensity in terms of their axis ratio in Fig. 1c seems far more plausible.

3. Data

a. Filtered data

The filtered data shown in Fig. 1c can now be examined in terms of the distribution of axis ratio as a function of drop diameter. Examples of distributions for various diameter intervals are given in Figs. 2a–d. Superimposed on the graphs are Gaussian curves, which are fitted to each of the distributions. In all cases, the axis ratio distributions seem to follow Gaussian functions closely. This was found to be the case for all diameters from 1.5 up to 9.5 mm.

b. System effects

The distributions seen in Fig. 2 are largely due to natural changes in drop axis ratios around their mean shapes. Nevertheless, when trying to derive the true

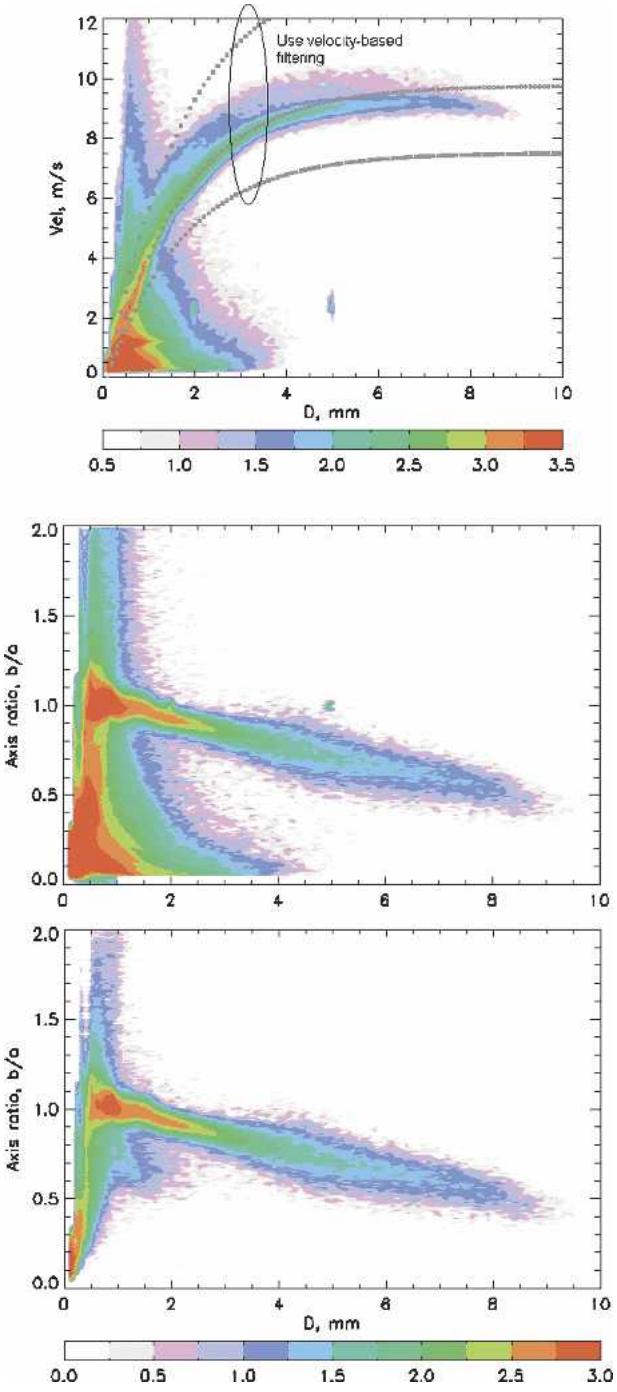

FIG. 1. (a) Velocity-based filter for the drop measurements, depicted on a color intensity plot on a logarithmic ($\log_{10}$) scale. (b) Drop axis ratios for all measured drops. (c) Drop axis ratios after removing mismatched drops. The color scale represents (a) $\log_{10}[N(D_e, v)]$, (b),(c) $\log_{10}[N(D_e, b/a)]$, where $N(D_e, v)$ is the number of drops with equivalent diameter D_e and velocity v, both within the instrument resolution intervals, and $N(D_e, b/a)$ is the number of drops with equivalent diameter D_e and axis ratio b/a, once again both within the instrument resolution intervals.

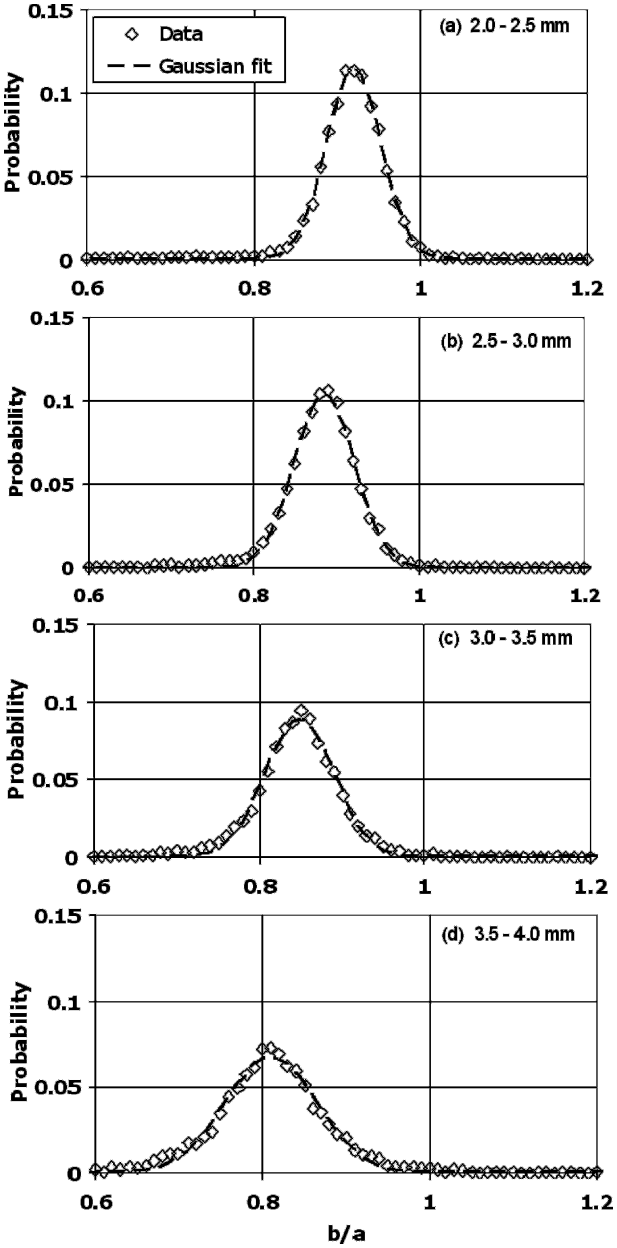

FIG. 2. Axis ratio distributions for various diameter intervals together with their Gaussian-fitted curves.

distributions from the experimental data, we need to consider the effect of the instrument itself, which, if nonnegligible, will contribute toward the overall spread in the observations. To remove the spreading due to the instrument, calibration spheres of precisely known size were dropped from an appropriate height, so that the spheres would reach similar terminal velocities corresponding to the equivalent rain drop diameter.

The spread of axis ratios measured using the calibration spheres are shown as intensity plots in Fig. 3 on an

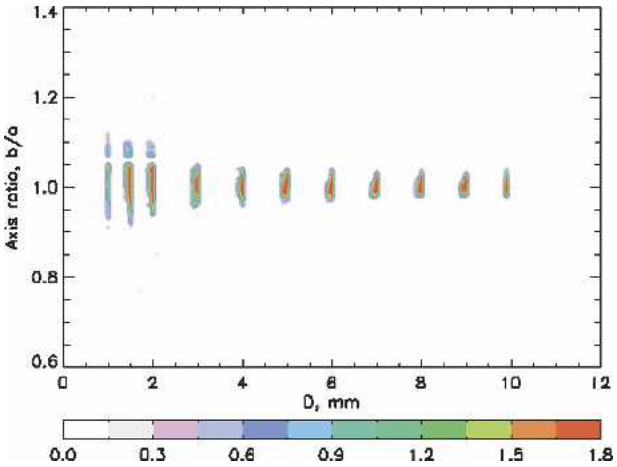

FIG. 3. Axis ratio distributions measured for calibration spheres, displayed in terms of the $\log_{10}$ $[N(D_e, b/a)]$ color scale.

enlarged scale. The spread is finite and seems to be diameter dependent, getting narrower at larger diameters. For all diameter intervals, the system spread was much narrower than that of the 80-m drop data. As an example, Fig. 4 compares the axis ratios of the calibration spheres with the experimental data for the diameter interval of 4–4.5 mm. The former has a peak at around 1 (i.e., spheres) and is much sharper than the 80-m drop data. Nevertheless, the system spread had to be removed from the experimental data to obtain more precise estimates of the drop axis ratio distributions. This is done by deconvolving the distributions of the experimental data by the system spread for each diameter interval.

As with the experimental data, the axis ratio distributions for the calibration spheres seemed to fit Gaussian functions accurately. For all diameter intervals ex-

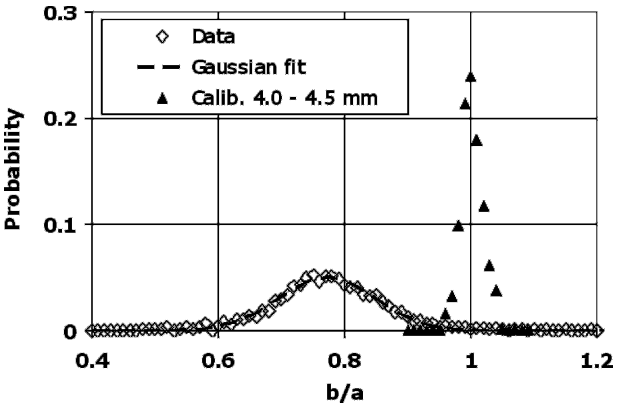

FIG. 4. Axis ratio distribution for drop diameter range 4–4.5 mm compared with the corresponding "point-spread function" from calibration spheres.

cept for the last (i.e., largest) one, the Gaussian fits gave mean values that were marginally larger than 1. The deconvolution was performed using the Gaussian-fitted functions for both the experimental data and the point spread function of the 2DVD. If we denote these two functions as $f^m(r)$ and $g(r)$, then the real axis ratio distribution $f^t(r)$ is related by

$$f^m(r) = f^t(r) * g(r), \quad (1)$$

where the symbol * represents convolution. The estimation of $f^t(r)$ was done by deconvolution using Fourier transform in the following manner:

1) Fourier transform Gaussian fit to the experimental data,
2) Fourier transform the Gaussian fit to the calibration curve, and
3) Inverse Fourier transform the ratio of 1) and 2).

The effect of the overall deconvolution process is to reduce slightly (albeit by a very small amount) the mean of the experimental data distributions for diameters up to 6 mm only. However, the reduction in standard deviation is more significant, as expected (not shown here). The results are given in Table 1 for all the diameter intervals. They are represented by the mean and the standard deviations of the deconvolved spectra.

4. Results and comparisons

a. Mean and standard deviation

Table 1 shows the expected decrease in the mean of the axis ratio distribution with increasing diameter. The data for the smallest diameter interval (1–1.5 mm) is not expected to be sufficiently accurate because of residual mismatch problems and the limited vertical resolution of the instrument, but for larger diameters this problem does not arise. We have seen that the distributions in all cases can be fitted to Gaussian shapes, but what is somewhat unexpected is that the standard deviation shows a noticeable increase in the 3–5-mm range from 0.04 to 0.08. Previous work on axis ratios using airborne particle measuring system (2D-PMS) probe data taken in rain showers showed the average standard deviation in the 2–6 mm range to be 0.068 (Chandrasekar et al. 1988). Note that our standard deviations for drops smaller than 3.5 mm are about half this value.

TABLE 1. Mean and standard deviation of Gaussian functions fitted to the deconvolved axis ratio distributions.

Diameter interval	Mean axis ratio	Std dev
1.0–1.5	0.98	0.036
1.5–2.0	0.948	0.037
2.0–2.5	0.911	0.028
2.5–3.0	0.881	0.031
3.0–3.5	0.844	0.037
3.5–4.0	0.808	0.050
4.0–4.5	0.771	0.073
4.5–5.0	0.732	0.081
5.0–5.5	0.704	0.077
5.5–6.0	0.671	0.071
6.0–6.5	0.645	0.072
6.5–7.0	0.617	0.071
7.0–7.5	0.589	0.075
7.5–8.0	0.553	0.068
8.0–8.5	0.520	0.070
8.5–9.0	0.474	0.065
9.0–9.5	0.446	0.067
9.5–10.0	0.424	

b. Comparisons

Here we compare the mean value of the axis ratio with some representative formulas quoted in the literature. Among them are

1) Pruppacher and Beard (1970, hereafter PB),
2) Beard and Chuang (1987, hereafter BC),
3) Andsager et al. (1999, hereafter ABL), and
4) Goddard et al. (1994b, hereafter RAL).

These have been approximated to various polynomials, as follows:

$$\frac{b}{a} = 1.03 - 0.062(D), \quad (2)$$

$$\frac{b}{a} = 1.0048 + 5.7 \times 10^{-4}(D) - 2.628 \times 10^{-2}(D^2) + 3.682 \times 10^{-3}(D^3) - 1.677 \times 10^{-4}(D^4), \quad (3)$$

$$\frac{b}{a} = 1.012 - 0.01445(D) - 1.028 \times 10^{-2}(D^2), \quad (4)$$

$$\frac{b}{a} = 1.075 - 6.5 \times 10^{-2}(D) - 3.6 \times 10^{-3}(D^2) + 4.0 \times 10^{-3}(D^3). \quad (5)$$

Equation (2) is a linear fit to wind tunnel data of PB ($1 \le D \le 9$ mm), (3) is a polynomial fit to the numerical model of BC ($1 \le D \le 7$ mm), (4) is a quadratic fit to laboratory and aircraft measurements ($1 \le D \le 4$ mm), and (5) is inferred from dual-polarized radar and Joss disdrometer comparisons ($1 \le D \le 5$ mm).

The comparisons are shown in Fig. 5a for 1–5 mm, and Fig. 5b for diameters greater than 5 mm. Note that the formula recommended by ABL is only valid up to

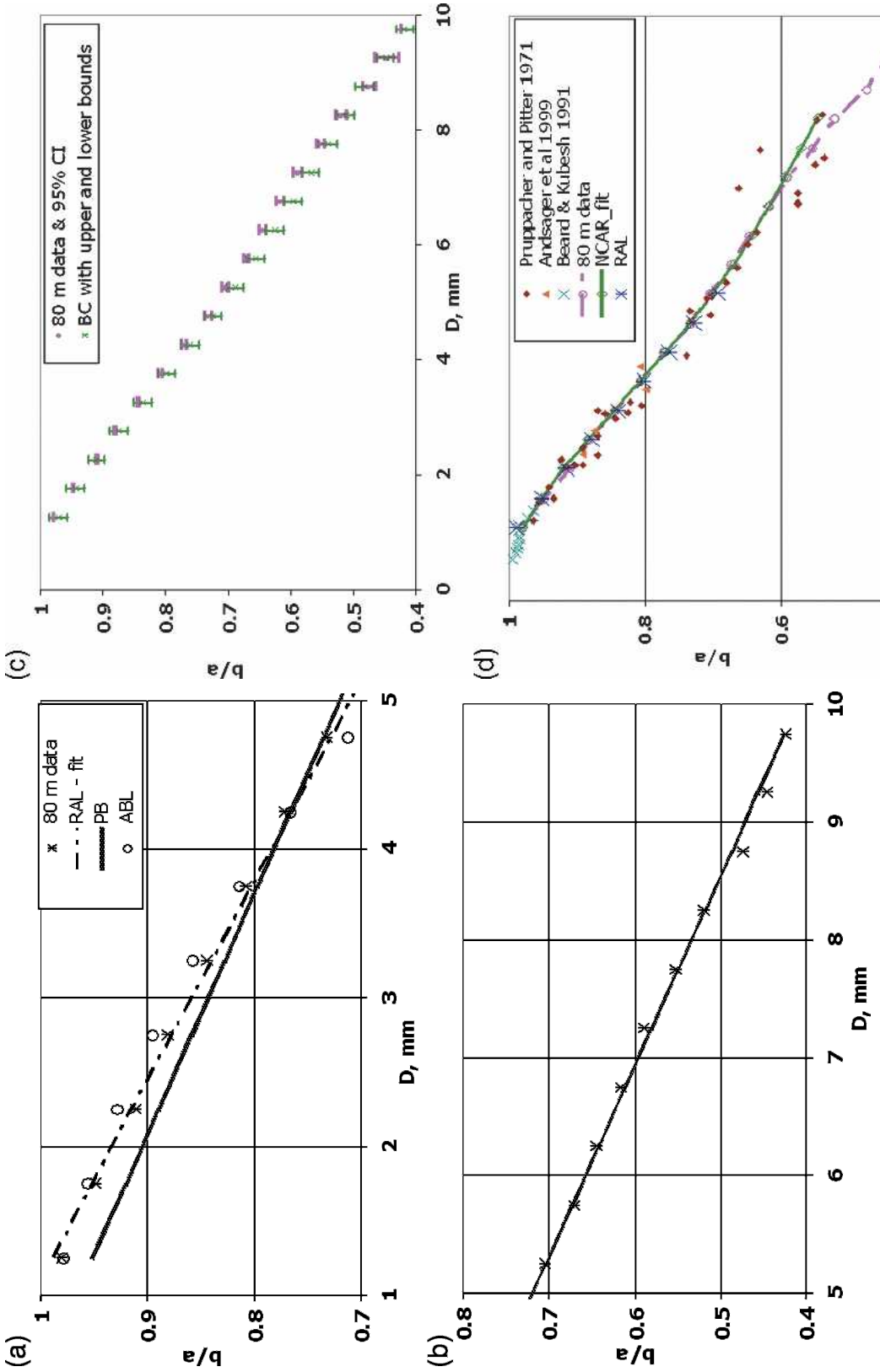

FIG. 5. Mean axis ratios compared with model formulas (a) $1 \le D \le 5$ mm and (b) $5 \le D \le 10$ mm. (c) Mean and 95% confidence interval compared with the upper and lower bounds of BC for $1 \le D \le 10$ mm. (d) Mean compared with published data and the NCAR formula.

4 mm and hence is not included in Fig. 5b. Also, the comparison with the numerical model of BC is given later.

Based on Fig. 5a, the following observations can be made: (i) the RAL fit is closest to the bridge data for 1–5 mm; (ii) the PB fit falls below the bridge data for $D < 4$ mm, with the difference increasing for smaller drops; this systematic increase toward sphericity has been noted in previous studies and attributed to drop oscillations; (iii) the ABL fit tends to overestimate the axis ratio relative to the bridge data in the range 2–3.5 mm. From Fig. 5b, it appears that the PB fit is a close fit to the bridge data over the entire big drop range (5–10 mm).

Next, we compare the bridge data with the numerical model described by BC, including their lower and upper bounds. Beard and Chuang (1987) calculated these bounds by including the variation in pressure distribution with Reynolds number and drop distortion. Figure 5c compares the BC calculation with the mean and 95% confidence interval (CI) from the bridge data. The bridge results (including the 95% CI) tend to consistently fall closer to the upper bound of the BC model, which is consistent with the RAL formula for $D \leq 5$ mm. The consistency between the bridge results and the RAL adjustment together with the BC model predictions indicates that the drops generated by the open hose (artificial rain shaft) are probably representative of those in natural rain.

Another formula quoted in the literature (Brandes et al. 2002) was empirically derived by combining drop shape observations by various authors and fitting a fourth-order polynomial for the mean axis ratio–diameter relationship:

$$\frac{b}{a} = 0.9951 + 2.51 \times 10^{-2}\,(D) - 3.644 \times 10^{-2}\,(D^2) + 5.303 \times 10^{-3}\,(D^3) - 2.492 \times 10^{-4}\,(D^4). \quad (6)$$

Figure 5d compares this equation [denoted as the National Center for Atmospheric Research (NCAR) fit] with the mean axis ratios from the bridge data. Also included are some of the published data used to derive the NCAR fit. The agreement up to 7 mm is excellent. It is indeed remarkable that the averaged fit to past laboratory and other measurements agrees so well with the mean axis ratios derived from the bridge experiment. It is also worth noting that the 2DVD enables the measurement and fast processing of large numbers of drops, several orders of magnitude larger than laboratory-based techniques.

Finally, we attempted our own fit to the 80-m data to various polynomial equations; however, no improvement was seen until a fourth-order equation given by

$$\frac{b}{a} = 0.9707 + 4.26 \times 10^{-2}\,(D) - 4.29 \times 10^{-2}\,(D^2) + 6.5 \times 10^{-3}\,(D^3) - 3.0 \times 10^{-4}\,(D^4) \quad (7)$$

was fitted. This gave an rms error of 0.0003 for $1.5 \leq D \leq 8$ mm. Note that this is not very different from Eq. (6) above.

c. Linear fit

For some applications, it is useful to have a linear relationship between the mean axis ratio and drop diameter. This is particularly useful when inferring the rainfall rate from the specific differential phase ($K_{\rm dp}$) measured by a dual-polarization radar. As an example, if we assume the PB (wind tunnel) data, which can be approximated to the linear relationship:

$$\frac{b}{a} = 1.03 - 0.062\,D; \quad 1 \leq D \leq 9 \text{ mm}, \quad (8)$$

this will lead to the relationship:

$$K_{dp} = \left(\frac{180}{\lambda}\right) 10^{-3}\,C\,W\,(0.062 D_m)^\circ \text{ km}^{-1}, \quad (9)$$

where 0.062 mm^{-1} is the gradient obtained from the mean axis ratio–diameter formula, C is a dimensionless constant (≈3.75 for Rayleigh scattering), W is the rainwater content in grams per cubic meter, D_m is the mass-weighted mean diameter in mm, and λ is the wavelength in meters (Jameson, 1985 or see section 7.1 of Bringi and Chandrasekar 2001). Equation (9) shows that $K_{\rm dp}$ can be simply related to the product WD_m, independent of the form of the DSD and the form of the axis ratio distribution if the mean axis ratio versus drop diameter is linear.

A linear relation of the form

$$\frac{b}{a} = 1 - \beta_{\rm eff}\,D \quad (10)$$

has been used to adjust the polarimetric rainfall algorithms, to take into account perturbations in drop shapes or orientations (Gorgucci et al. 2002). The R-$K_{\rm dp}$ power-law estimator will, for example, have the multiplicative coefficient nearly proportional to the inverse of $\beta_{\rm eff}$.

Here, we have attempted a similar linear fit to our results of the mean axis ratio versus diameter. If we use only the data range in which we have reasonable confidence (i.e., 1.5–8 mm), then the linear fit

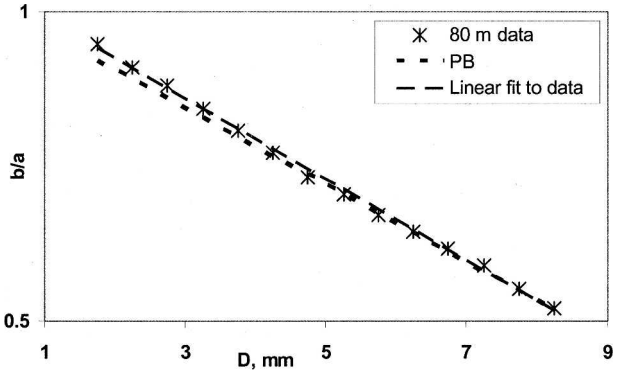

FIG. 6. Linear fit to the bridge data compared with PB model for $1.5 \leq D \leq 8$ mm.

$$\frac{b}{a} = 1.055 - 0.0653\,D \quad \text{for} \quad 1.5 \leq D \leq 8 \text{ mm} \tag{11}$$

gives a good approximation. This is compared with the PB linear approximation in Fig. 6. Our fit shows a sharper gradient, but this does not imply that the drops are more oblate than the PB shapes. For $D \leq 1.5$ mm, a fit to the laboratory data of Kubesh and Beard (1993) is recommended since as seen from Fig. 5d, our data merges well at $D = 1.5$ mm.

d. Fall velocity comparisons

Earlier it was mentioned that drops that were mismatched by the two cameras of the video disdrometer were eliminated using a velocity-based filtering technique (Fig. 1a) that subsequently lead to more plausible distributions of axis ratios. The same filtered dataset was used to derive the mean of the fall velocity distributions for the same diameter intervals as before.

The mean fall velocity is compared with the Gunn–Kinzer (1949, hereafter GK) data as well as the fitted formula by Atlas et al. (1973) in Fig. 7. The bridge data includes the corresponding 95% confidence interval. A minor adjustment had to be made for the GK curves to take into account the terrain height of the location at which the bridge experiment was conducted. Assuming a *U.S. Standard Atmosphere, 1976,* the air density was calculated for the terrain height of 480 m above MSL, which was then used to calculate the corresponding correction factor for the fall speed using,

$$v(h) = \left[\frac{\rho_0}{\rho(h)}\right]^m v_0, \tag{12}$$

where ρ_0 and $\rho(h)$ are the air density at ground level at height h, respectively, v_0 is the drop terminal velocity at sea level, and m is typically 0.4 (Foote and du Toit 1969). For better accuracy, m is set to a diameter dependent expression given by (Beard 1985):

$$m(D) = 0.375 + 0.025D. \tag{13}$$

This results in a 1.8% increase in fall speed for 1-mm drop (an increase because of the more rarified atmosphere). Comparisons show excellent agreement for drop diameters up to 6 mm. Gunn and Kinzer (1949) data are not available beyond that but the Atlas et al. (1973) fitted formula reaches a plateau, while our data shows a slight tendency toward decreasing velocity with increasing diameter for the large drops. It is not clear why such a decrease should occur, but one possible reason is that for drops larger than 6.5 mm, the drag increases due to increased distortion when compared with the increase in weight. Some observations in the past have also reported a similar trend. Laws (1941) used previously published data on fall velocity measured in natural rain conditions showing that in drops for diameters larger than 5.5 mm, the terminal velocity decreases with increasing size. The decrease in velocity has also been evident in the adjusted velocities aloft, as seen in Fig. 6 of Beard (1976).

Brandes et al. (2002) have proposed a fit based on GK data as well as Beard and Pruppacher (1969) measurements up to 8 mm, given by

$$v = -0.1021 + 4.932(D) - 0.9551\,D^2 + 0.07934\,D^3 - 0.002362\,D^4. \tag{14}$$

Figure 7 includes the results from this expression. The bridge data show excellent agreement with this formula for D up to 8 mm, including the slight decreasing tendency in fall velocity for drops larger than 7 mm.

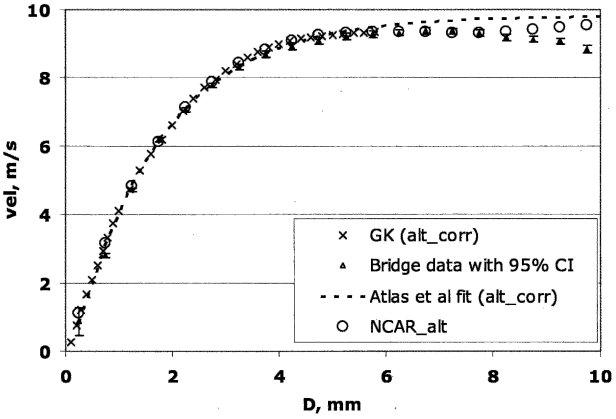

FIG. 7. Mean velocity from the bridge data vs D compared with GK data and the empirical formula from Atlas et al. (1973). Also shown is the fit using (14), denoted by NCAR_alt. In all cases, an altitude adjustment is made for the fall speed.

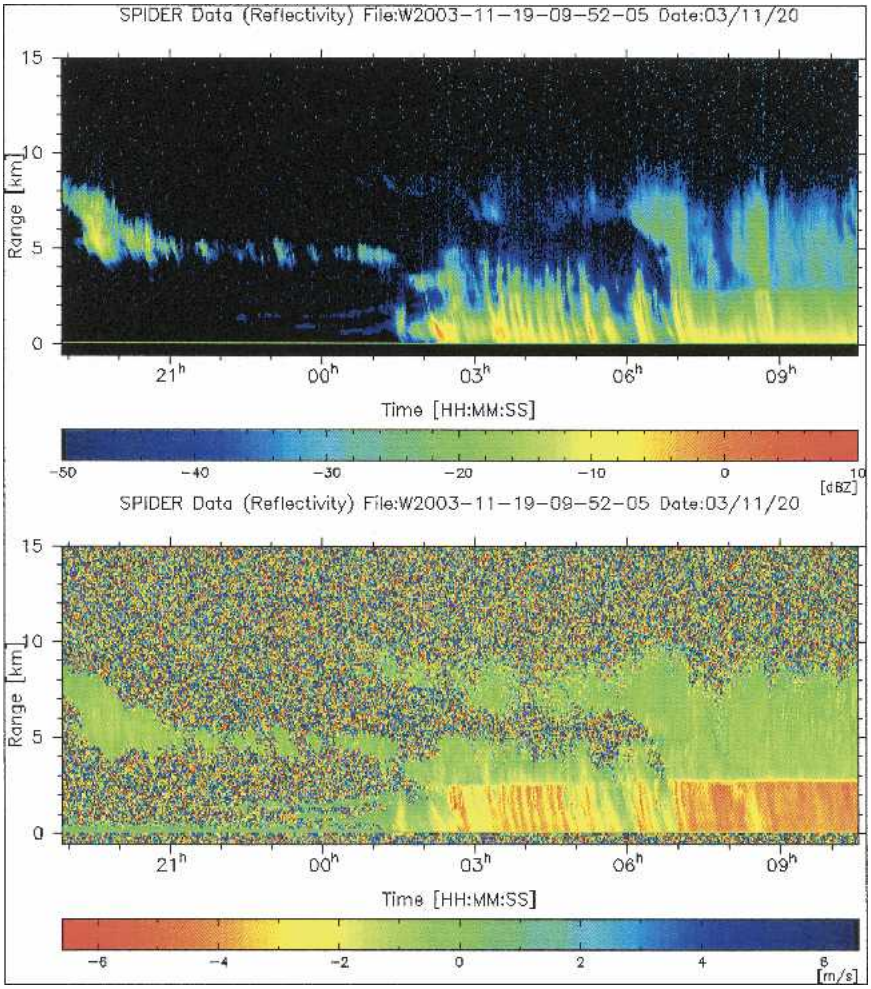

FIG. 8. Vertically pointing W-band radar data used to classify events: (top) reflectivity and (bottom) velocity.

5. Drop shape data in (midlatitude) stratiform rain

The results and comparisons shown so far correspond to artificially generated drops falling in still air conditions. In this section, we compare these results with observations taken in low-intensity stratiform rain. The data were obtained using another 2DVD, a unit that is similar in configuration to the one used in the bridge experiment. It is installed on the roof top of a four-story building in Koganei, Tokyo (latitude: 35.71°, longitude: 139.49°). This unit was calibrated and installed during the latter half of 2003 and has been continuously measuring the characteristics of hydrometeors. A vertically pointing 95-GHz Doppler radar is conveniently collocated, which is also operated continuously. Data from this W-band system were used to classify precipitation events.

Two events were selected for this study, as follows:

1) 0000–1600 (local time, JST) 11 November 2003, and
2) 0400–1200 (local time, JST) 20 November 2003.

In both cases, the radar data showed clearly a sharp increase in the mean Doppler velocity at the transition from snow to rain. In the case of event 1, this height (identified by a sharp increase in the fall velocity of hydrometeors) was located at 2.9 km while for case 2, the height was slightly lower at 2.7 km. On example is shown in Fig. 8, which illustrates the clear change in Doppler velocity for case 2. The rainfall rates in both cases did not exceed 10 mm h^{-1} and for most of the time, were below 5 mm h^{-1}.

The 2DVD data for these two events were combined and analyzed in the same way as the bridge data. Figures 9a,b show the measured drop axis ratios with and without the velocity-based filtering. Once again, the filtering process is seen to remove most of the mismatched drops.

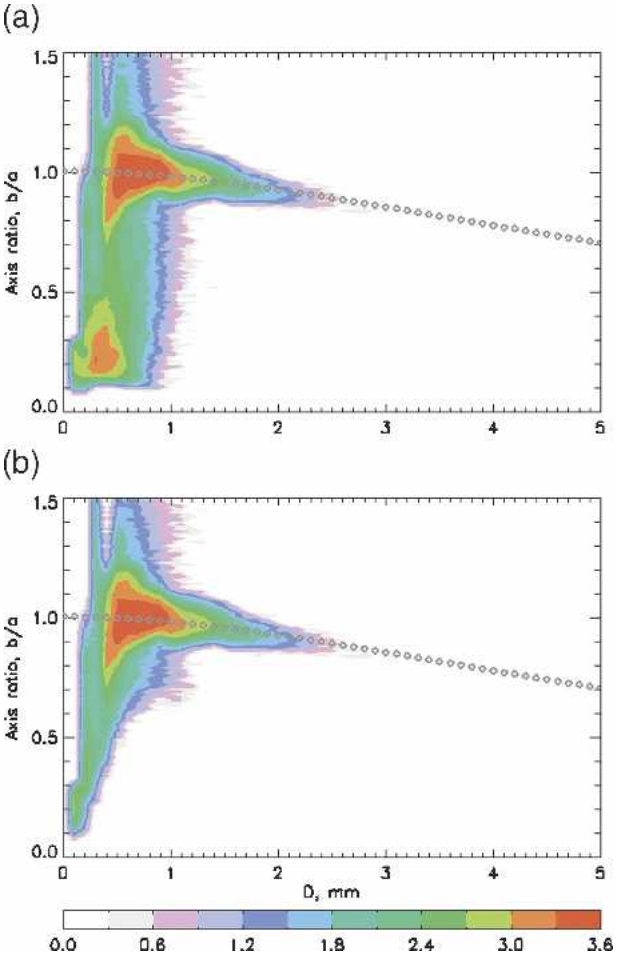

FIG. 9. Drop axis ratios from Koganei (Tokyo) measurements, displayed in terms of $\log_{10}$ [$N(D_e, b/a)$] color scale: (a) for all measured drops and (b) after removing mismatched drops.

The axis ratio distributions were derived for the same diameter intervals as before and the instrument spread was deconvolved using the procedure described earlier. The mean of the resulting distributions are compared with those of the bridge data in Table 2. They agree to within 1% of each other but as seen in Fig. 9b, there were not many drops larger than 3 mm. In fact, in the 3–3.5-mm interval, the total number of drops was only 19. For the smaller drops (i.e., in the 1–3-mm range) the agreement between the two sets of data is close (see Fig. 10 for an example of axis ratio distributions), indicating that that the drop shapes in the bridge experiment closely resemble those of drops occurring in natural rain, in spite of the vastly different rain rates.

TABLE 2. Gaussian-fitted mean axis ratios for Koganei (Tokyo) stratiform rain data compared with the Bridge data.

Diameter mm^{-1}	1.25	1.75	2.25	2.75	3.25
Koganei	0.99	0.95	0.9083	0.8747	0.855
Bridge (80 m)	0.98	0.948	0.911	0.881	0.844

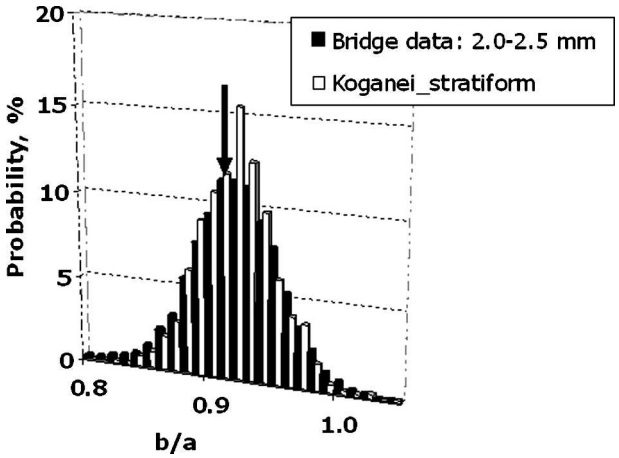

FIG. 10. Distributions of axis ratios from Bridge data and Koganei (Tokyo) data for the diameter interval range 2.0–2.5 mm. Arrow shows the BC model axis ratio.

6. Drop oscillations

The distribution of axis ratio observed from the bridge data is indicative of drop oscillations, even after considering the finite-diameter interval over which these distributions were calculated. Four examples of the axis ratio distributions are shown in Fig. 11. Also included are the BC mean for the center of the diameter interval and for the corresponding lower and upper limits. The BC equilibrium axis ratios lie within the axis ratio distribution, although the mean of the observation in each case is a few percent higher than the BC mean and closer to the upper bound of the BC model. Because of the nearly symmetric scatter about the BC mean, the inferred mode of oscillation appears to be dominated by the oblate–prolate axisymmetric mode (Kubesh and Beard 1993). This applies for all drop sizes from 1.5–9 mm in the bridge data. Pure transverse mode oscillations (normally associated with one-sided, asymmetric distributions and observed for $D \sim 1.0$–1.3 mm by Beard et al. 1991) are not evident in any of our histograms.

Past laboratory measurements for $D \sim 1.4$–4.0 mm (Kubesh and Beard 1993; Andsager et al. 1999) have shown axis ratio distributions both relatively symmetric as well as relatively asymmetric about the BC model mean, depending on the drop size interval considered as well as the method of drop generation. In contrast, the bridge data (for $D > 1.5$ mm) show axis ratio dis-

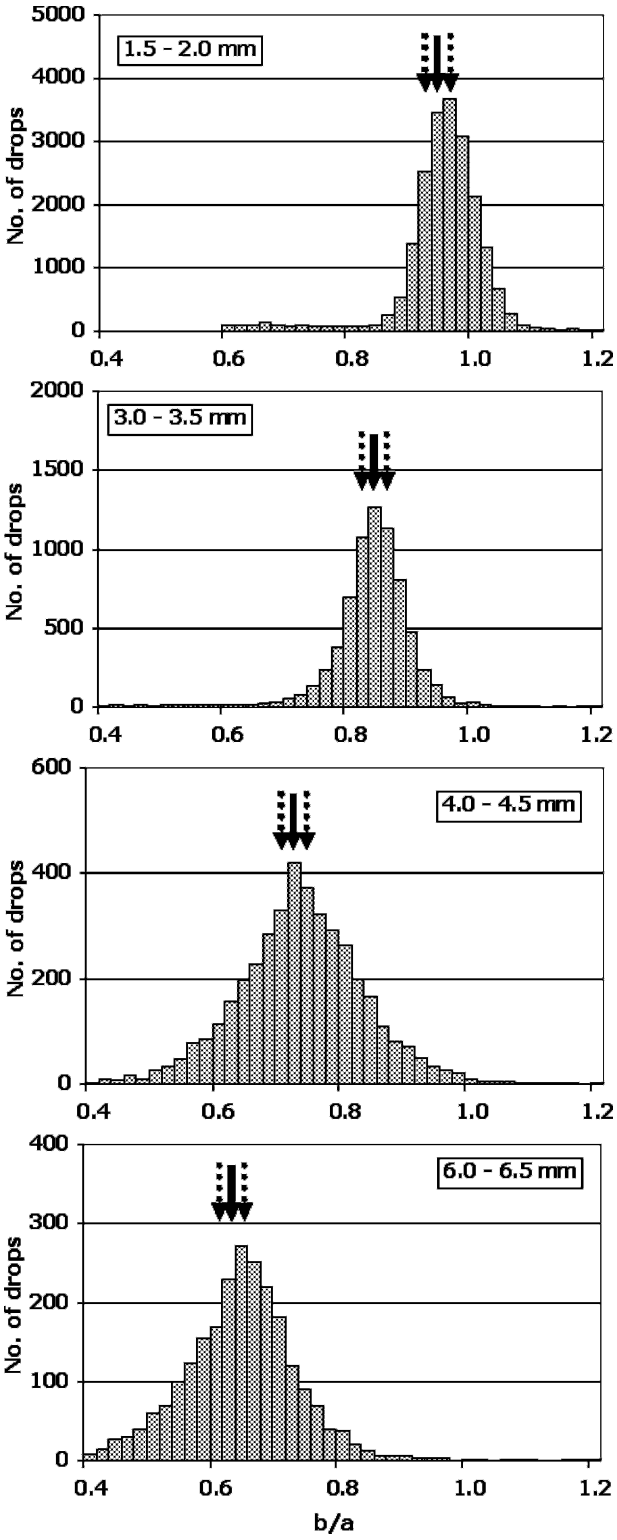

FIG. 11. Axis ratio distributions for various diameter intervals. (The solid arrow indicates the BC equilibrium shape value for the mean diameter and the dotted arrows indicate those for the upper and lower diameters.)

tributions that are clearly more symmetric than asymmetric about the BC model mean. The difference in axis ratio distributions between past laboratory and the present bridge data could be, in part, due to the big difference in fall distance (27 versus 80 m) and/or the method of drop generation. The 80-m fall distance used in this experiment is thought to be sufficient to ensure that the drops reach their steady-state oscillation mode, irrespective of the initial conditions. Furthermore, the number of drops measured in our experiment was higher (by two to three orders of magnitude) compared with the previous laboratory studies, leading to statistically more representative histograms of the axis ratio distributions.

Tokay and Beard (1996) in their field study concluded that "... aerodynamic forcing through positive feedback from the drag to the oblate–prolate mode is suggested to produce continuous oscillations for raindrops of all sizes having larger amplitudes for larger rain drops." The bridge results support their conclusions in terms of both the mode of oscillation and the increase in oscillation amplitude with drop size.

Another explanation for the apparent lack of transverse mode oscillations could be related to the high concentration of drops in our artificial rain shaft, which increases the probability of drop collisions. For a given energy input, the oblate–prolate mode has much higher amplitudes than all other modes thus making it difficult to detect the component of the transverse mode in the bridge data (Beard and Kubesh 1991). Even so, our analysis of the stratiform rain data from Koganei (where collisional forcing is unlikely) does not show any clear evidence of transverse mode oscillations being present, that is, the mean axis ratios in Table 2, are within 1% of the bridge data, and the example distributions as shown in Fig. 10 are similar to each other.

7. Summary

We have reported the results of an experiment in which water was sprayed from a bridge at a height of 80 m under calm conditions, and the characteristics of the drops so generated were measured using a 2DVD at ground level. The shapes and velocities of individual drops in the 1–10-mm size range were analyzed as a function of the equivolumetric drop diameter. Using a velocity-based filtering method, it was possible to eliminate the problem of mismatched drops. Even after filtering, the total number of drops measured was around 115 000.

Histograms of axis ratio were obtained for drop diameters ranging from 1 to 9 mm. These distributions were deconvolved by the point-spread function of the

instrument for each of the diameter interval range. The resulting axis ratio distributions were Gaussian in shape with standard deviation generally increasing with drop diameter. The symmetric shape of the distributions (with mean close to the upper bound of the Beard and Chuang equilibrium shape) showed the dominance of the oblate–prolate mode of oscillation for all drop diameter intervals from 1.5 to 9 mm. A significant component of the transverse mode of oscillation could not be detected in our axis ratio distributions for $D \geq 1.5$ mm. The 80-m fall distance is believed to be sufficient for steady-state oscillations to be reached irrespective of the initial conditions.

The axis ratio mean compares well with two empirically fitted formulas reported in the literature, one being inferred from radar disdrometer (Joss type) comparisons (Goddard et al. 1994b) and the other (Brandes et al. 2002) being determined by combining observations from wind tunnel, airborne, and laboratory data. Out of the two, the agreement with the latter is marginally better over the size range 1.5–7 mm.

Analyses were also carried out on data collected using another 2DVD during moderate stratiform precipitation events in a midlatitude location (Tokyo, Japan). The resulting axis ratio distributions were very similar to the bridge data for diameters up to 4 mm in spite of the vastly different drop concentration conditions. The dominant oscillation mode was once again inferred to be the oblate–prolate mode. For diameters larger than 4 mm, the number of drops in the stratiform rain events was too small to derive meaningful distributions. Although the bridge and the stratiform rain results were consistent with each other, further studies are needed to confirm or otherwise the applicability of the results to convective rain events.

Finally, fall velocity distributions as measured by the 2DVD were analyzed from the bridge experiment. The mean velocity results are in close agreement with GK data for diameters up to 5 mm, after a small adjustment to take into account the height of the experiment location. More interestingly, our results show excellent agreement with a previously published fourth-order fit based not just on GK data but also on Beard and Pruppacher (1969) data, which ranges up to 8-mm drop diameter, including a decreasing trend in terminal velocity with increasing diameter for large drops above 6 mm, thought to be owing to the increase in drag due to drop distortion being large compared with the corresponding increase in weight.

Acknowledgments. This work was supported by the National Science Foundation via Grant ATM-0140350. The authors are grateful to Michael Schöenhuber and Gunther Lammer of Joanneum Research for their thorough and precise conduct of the experiments, and to Prof W. L. Randeu for supporting and recommending the Jauntal Bridge for the experiments. The Koganei 2DVD data were kindly provided by Hiroshi Hanado, and the W-band radar data were made available by Dr. Y. Ohno both of NICT, Japan.

REFERENCES

Allnutt, J., 1989: *Satellite-to-Ground Radiowave Propagation.* Peter Peregrinus, Ltd., 421 pp.

Andsager, K., K. V. Beard, and N. F. Laird, 1999: Laboratory measurements of axis ratios for large raindrops. *J. Atmos. Sci.,* **56,** 2673–2683.

Atlas, D., R. C. Srivastava, and R. S. Sekkon, 1973: Doppler radar characteristics of precipitation at vertical incidence. *Rev. Geophys. Space Phys.,* **2,** 1–35.

Beard, K. V., 1976: Terminal velocity and shape of cloud and precipitation drops aloft. *J. Atmos. Sci.,* **33,** 851–864.

——, 1985: Simple altitude adjustments for raindrop velocities for Doppler radar analysis. *J. Atmos. Oceanic Technol.,* **2,** 468–486.

——, and H. R. Pruppacher, 1969: A determination of the terminal Velocity and drag of small water drops by means of a wind tunnel. *J. Atmos. Sci.,* **26,** 1066–1072.

——, and C. Chuang, 1987: A new model for the equilibrium shape of raindrops. *J. Atmos. Sci.,* **44,** 1509–1524.

——, and R. J. Kubesh, 1991: Laboratory measurements of small raindrop distortion. Part II: Oscillation frequencies and modes. *J. Atmos. Sci.,* **48,** 2245–2264.

——, ——, and H. T. Ochs, 1991: Laboratory measurements of small raindrop distortion. Part I: Axis ratios and fall behavior. *J. Atmos. Sci.,* **48,** 698–710.

Brandes, E. A., G. Zhang, and J. Vivekanandan, 2002: Experiments in rainfall estimation with a polarimetric radar in a subtropical environment. *J. Appl. Meteor.,* **41,** 674–684.

Bringi, V. N., and V. Chandrasekar, 2001: Polarisation Doppler Weather Radar. Cambridge University Press, 636 pp.

Chandrasekar, V., W. A. Cooper, and V. N. Bringi, 1988: Axis ratios and oscillations of raindrops. *J. Atmos. Sci.,* **45,** 1323–1333.

Foote, G. B., and P. S. du Toit, 1969: Terminal velocity of raindrops aloft. *J. Appl. Meteor.,* **8,** 245–253.

Goddard, J. W. F., and S. M. Cherry, 1984: The ability of dual-polarization radar (co-polar linear) to predict rainfall rate and microwave attenuation. *Radio Sci.,* **19,** 201–208.

——, ——, and V. N. Bringi, 1982: Comparison of dual-polarization radar measurements of rain with ground-based disdrometer measurements. *J. Appl. Meteor.,* **21,** 252–256.

——, J. D. Eastment, and M. Thurai, 1994a: The Chilbolton advanced meteorological radar: A tool for multidisciplinary atmospheric research. *IEE Electron. Comms. Eng. J.,* **6** (2), 77–86.

——, ——, and J. Tan, 1994b: Self-consistent measurements of differential phase and differential reflectivity in rain. *Proc. 1994 Int. Geoscience and Remote Sensing Symp.*, Pasadena, CA, IEEE, 369–371.

Gorgucci, E., V. Chandrasekar, V. N. Bringi, and G. Scarchilli, 2002: Estimation of raindrop size distribution parameters from polarimetric radar measurements. *J. Atmos. Sci.,* **59,** 2373–2384.

Gunn, R., and G. D. Kinzer, 1949: The terminal velocity of fall for water droplets in stagnant air. *J. Meteor.,* **6,** 243–248.

Jameson, A. R., 1985: Microphysical interpretation of multiparameter radar measurements in rain. Part III: Interpretation and measurements of propagation differential phase shift between orthogonal linear polarizations. *J. Atmos. Sci.,* **42,** 607–614.

Kruger, A., and W. F. Krajewski, 2002: Two-dimensional video disdrometer: A description. *J. Atmos. Oceanic Technol.,* **19,** 602–617.

Kubesh, R. J., and K. V. Beard, 1993: Laboratory measurements of spontaneous oscillations for moderate-size raindrops. *J. Atmos. Sci.,* **50,** 1089–1098.

Laws, J. O., 1941: Measurements of the fall velocity of water drops and rain drops. *Hydrology,* **22,** 709–721.

Pruppacher, H. R., and K. V. Beard, 1970: A wind tunnel investigation of the internal circulation and shape of water drops falling at terminal velocity in air. *Quart. J. Roy. Meteor. Soc.,* **96,** 247–256.

——, and R. L. Pitter, 1971: A semi-empirical determination of the shape of cloud and rain drops. *J. Atmos. Sci.,* **28,** 86–94.

——, and K. V. Klett, 1997: *Microphysics of Clouds and Precipitation.* 2d ed. Kluwer Academic, 954 pp.

Randeu, W. L., M. Schönhuber, and G. Lammer, 2002: Real-time measurements and analyses of precipitation micro-structure and dynamics. *Proc. of ERAD (2002)*, Delft, Netherlands, Eur. Geophys. Soc., 78–83.

Schönhuber, M., H. Urban, J. P. V. Poires Baptista, W. L. Randeu, and W. Reidler, 1997: Weather radar versus 2D-videodistrometer data. *Weather Radar Technology for Water Resources Management*, B. Braga Jr. and O. Massambani, Eds., UNESCO Press, 159–171.

Tokay, A., and K. L. Beard, 1996: A field study of raindrop oscillations. Part I: Observation of size spectra and evaluation of oscillation causes. *J. Appl. Meteor.,* **35,** 1671–1687.

——, A. Kruger, and W. Krajewski, 2001: Comparison of drop size distribution measurements by impact and optical disdrometers. *J. Appl. Meteor.,* **40,** 2083–2097.